NANO LETTERS

Letter

pubs.acs.org/NanoLett

Encoding Active Device Elements at Nanowire Tips

You-Shin No,[†,‡] Ruixuan Gao,[†] Max N. Mankin,[†] Robert W. Day,[†] Hong-Gyu Park,[*,‡] and Charles M. Lieber[*,†,§]

[†]Department of Chemistry and Chemical Biology, Harvard University, Cambridge, Massachusetts 02138, United States

[‡]Department of Physics, Korea University, Seoul 136-701, Republic of Korea

[§]Harvard John A. Paulson School of Engineering and Applied Sciences, Harvard University, Cambridge, Massachusetts 02138, United States

Supporting Information

ABSTRACT: Semiconductor nanowires and other one-dimensional materials are attractive for highly sensitive and spatially confined electrical and optical signal detection in biological and physical systems, although it has been difficult to localize active electronic or optoelectronic device function at one end of such one-dimensional structures. Here we report a new nanowire structure in which the material and dopant are modulated specifically at only one end of nanowires to encode an active two-terminal device element. We present a general bottom-up synthetic scheme for these tip-modulated nanowires and illustrate this with the synthesis of nanoscale p−n junctions. Electron microscopy imaging verifies the designed p-Si nanowire core with SiO_2 insulating inner shell and n-Si outer shell with clean p-Si/n-Si tip junction. Electrical transport measurements with independent contacts to the p-Si core and n-Si shell exhibited a current rectification behavior through the tip and no detectable current through the SiO_2 shell. Electrical measurements also exhibited an n-type response in conductance versus water-gate voltage with pulsed gate experiments yielding a temporal resolution of at least 0.1 ms and ∼90% device sensitivity localized to within 0.5 μm from the nanowire p−n tip. In addition, photocurrent experiments showed an open-circuit voltage of 0.75 V at illumination power of ∼28.1 μW, exhibited linear dependence of photocurrent with respect to incident illumination power with an estimated responsivity up to ∼0.22 A/W, and revealed localized photocurrent generation at the nanowire tip. The tip-modulated concept was further extended to a top-down/bottom-up hybrid approach that enabled large-scale production of vertical tip-modulated nanowires with a final synthetic yield of >75% with >4300 nanowires. Vertical tip-modulated nanowires were fabricated into >50 individually addressable nanowire device arrays showing diode-like current−voltage characteristics. These tip-modulated nanowire devices provide substantial opportunity in areas ranging from biological and chemical sensing to optoelectronic signal and nanoscale photodetection.

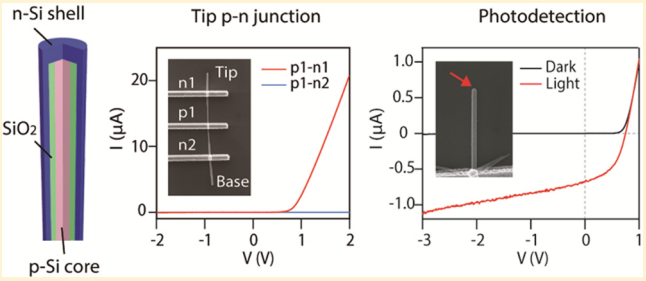

KEYWORDS: *One-dimensional nanostructure, p−n junction, nanodevice, potentiometric sensor, photodetector, wafer-scale nanodevices*

One-dimensional (1D) nanowires are promising as building blocks for devices capable of generating and detecting electrical and optical signals with high sensitivity and spatial resolution.[1−4] In particular, nanowires offer unique opportunities for probing biological systems because nanowires can be controllably synthesized into different morphologies with tunable electrical and optical properties.[5−11] For example, kinked Si nanowires with synthetically encoded nanoscale field effect transistors (FETs) demonstrated for the first time intracellular recording of action potentials in a minimally invasive manner.[7] Nanotubes integrated with nanoscale FETs have also shown the ability to record multiplexed intracellular signals from both single cells and networks of cells.[8,9] In addition, a point-like probe for both electrical and optical signals based on three-dimensional (3D) kinked p−n junction nanowires has been reported,[10] although efficient preparation of even modest size arrays of individually addressable detectors and multifunctional nanoprobes has remained challenging.

Here, we report a conceptually new method for modulating the composition and/or doping at only the tips of nanowires, termed tip-modulated nanowires. We illustrate this paradigm with the synthesis of p−n tip junctions. Characterization of the electrical and optical properties of devices configured from these new structures demonstrates the capability of tip-localized electronic and photonic detection. In addition, we generalize the concept to a hybrid top-down/bottom-up approach for large-scale production of vertical tip-modulated nanowires and show that it is possible to configure addressable tip-modulated vertical nanowire detector arrays.

Our tip-modulated nanowire structure (Figure 1a, right) combines the axial and radial modulation of nanowire doping and composition (Figure 1a, left) developed previously.[12−21]

Received: June 2, 2016
Revised: June 20, 2016
Published: June 23, 2016

DOI: 10.1021/acs.nanolett.6b02236
Nano Lett. 2016, 16, 4713−4719

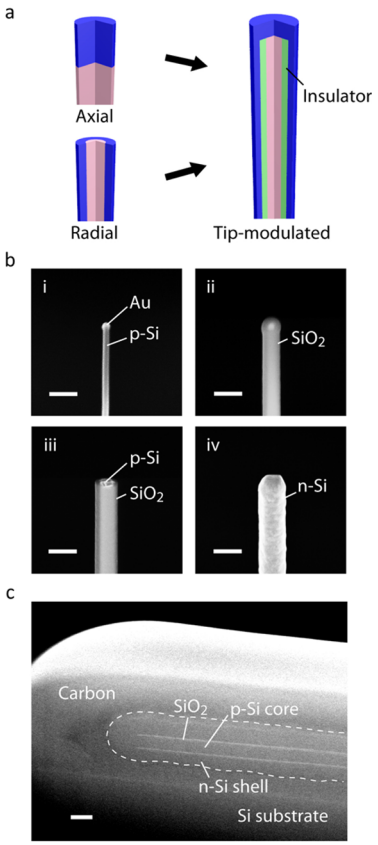

Figure 1. Tip-modulated nanowire concept, synthesis, and material characterization. (a) Schematic showing an axial (top left), radial core/shell (bottom left), and tip-modulated nanowire structures (right). (b) SEM images (45° tilt) of the same nanowire after each synthetic step: (i) Au nanoparticle-catalyzed growth of a p-Si nanowire core on a Si(111) substrate; (ii) deposition of SiO_2 by ALD; (iii) removal of the nanowire tip containing the Au nanoparticle by ultrasonication; and (iv) growth of the n-Si shell by CVD. Scale bars, 200 nm. (c) SEM image of a longitudinal cross-section of a tip-modulated p−n junction nanowire tip after focused ion beam (FIB) sectioning. Prior to FIB sectioning the nanowire was coated with an amorphous carbon protective layer; the carbon layer/nanowire boundary is highlighted by the white dashed line. Scale bar, 100 nm.

Axial dopant or composition modulation during nanowire growth can produce a localized junction at a specific position along a nanowire axis (Figure 1a, top left),[12,13,18−20] whereas the corresponding radial-modulation yields a core/shell structure and junction at the core/shell interface (Figure 1a, bottom left).[14−17,21] Our tip-modulated nanowire has a p-type core/insulator shell/n-type shell configuration in the radial direction but a p-type core/n-type axial interface at the tip, which yields the desired localized p−n junction (Figure 1a, right).

The synthetic protocol for our tip-modulated nanowires involves several key steps (Figure 1b, Supporting Information Figure S1a, see Materials and Methods in Supporting Information). First, p-Si nanowire cores are epitaxially grown on a Si(111) substrate via the Au nanoparticle-catalyzed vapor−liquid−solid (VLS) mechanism in a home-built chemical vapor deposition (CVD) chamber.[22−24] The growth substrate is coated with SiO_2 by atomic layer deposition (ALD) and then covered with SU-8 resist sufficiently thick to cover the vertical nanowires. The upper portion of the SU-8 is removed in an oxygen plasma to expose the nanowire tips, the exposed tips are removed in an ultrasonication bath, and then the remaining resist is completely removed in an oxygen plasma. Last, the p-Si nanowire tip is cleaned with a brief buffered hydrofluoric acid (BHF) etch, the substrate is quickly transferred back to the CVD reactor, and the n-Si shell is deposited.

Scanning electron microscopy (SEM) imaging reveals the nanowire structure following each key synthetic step as shown in Figure 1b. For example, the Au nanoparticle catalyst is visible at the nanowire tip following p-Si nanowire core growth (Figure 1b, i) and ALD SiO_2 shell deposition (Figure 1b, ii) due to the contrast differences between the Si core, SiO_2, and Au. These images further show that the nanowire diameter increases from ca. 50 to 130 nm following deposition of the SiO_2 shell. Next, the Au nanoparticle is absent and the length of the nanowire is reduced following the ultrasonication tip-removal step (Figure 1b, iii) as expected. Last and following n-Si deposition (Figure 1b, iv), the diameter increases to 200 nm consistent with the shell deposition. SEM images further show that the area of the exposed p-Si core tip can be increased through additional BHF etch (Supporting Information Figure S1b, iii′) and thus yield a larger area tip-modulated p−n junction following the n-Si shell deposition (Supporting Information Figure S1b, iv′).

In addition, we have used focused ion beam to section tip-modulated p−n junction structure along the nanowire axis (see Materials and Methods in Supporting Information). An SEM image of the cross-section (Figure 1c) reveals several important features. First, the SiO_2 layer between the p-Si core and n-Si shell extends along the nanowire and ends near the tip of nanowire as designed. Second, no interface or contrast is observed between the p-Si core and n-Si shell near the nanowire tip. These observations show that the core and shell are only connected at the tip with an estimated junction area of less than 10^{-14} m^2 assuming a circular cross section with diameter of ca. 50 nm. In addition, we carried out high-resolution transmission electron microscopy (TEM) to further characterize the junction interface of an as-synthesized nanowire (Supporting Information Figure S2). The TEM image shows continuous Si lattice fringes across the junction, consistent with results in Figure 1c. Taken together, the SEM and TEM characterization suggests that the synthesized structure matches the structural design (Figure 1a) of our tip-modulated nanowire.

To investigate the electrical transport properties of the synthesized tip-modulated nanowires, we shear-transferred nanowires to Si_3N_4 substrate and fabricated single nanowire devices with electrical contacts selectively defined to the p-Si core and n-Si shell (Supporting Information Figure S3, see Materials and Methods in Supporting Information).[14,15] Briefly, electron-beam lithography (EBL) was used to define SU-8 in order to etch selectively the n-Si shell and ALD deposited SiO_2 at one end opposite the tip using potassium hydroxide (KOH) and BHF solutions, respectively. A second step of EBL and metallization was used to define contacts to p-core and n-shell regions. SEM images (Figure 2a) show a representative device with one n-shell contact near the tip (red arrow), a p-core contact in the middle of the nanowire, and a second n-shell contact near the base (blue arrow). Higher-magnification SEM images of the tip and base show the n-Si shell termination at the tip end (Figure 2a, top right) and the insulating SiO_2 shell layer between p-Si core and n-Si shell at the base end (Figure 2a, bottom right).

DOI: 10.1021/acs.nanolett.6b02236
Nano Lett. 2016, 16, 4713−4719

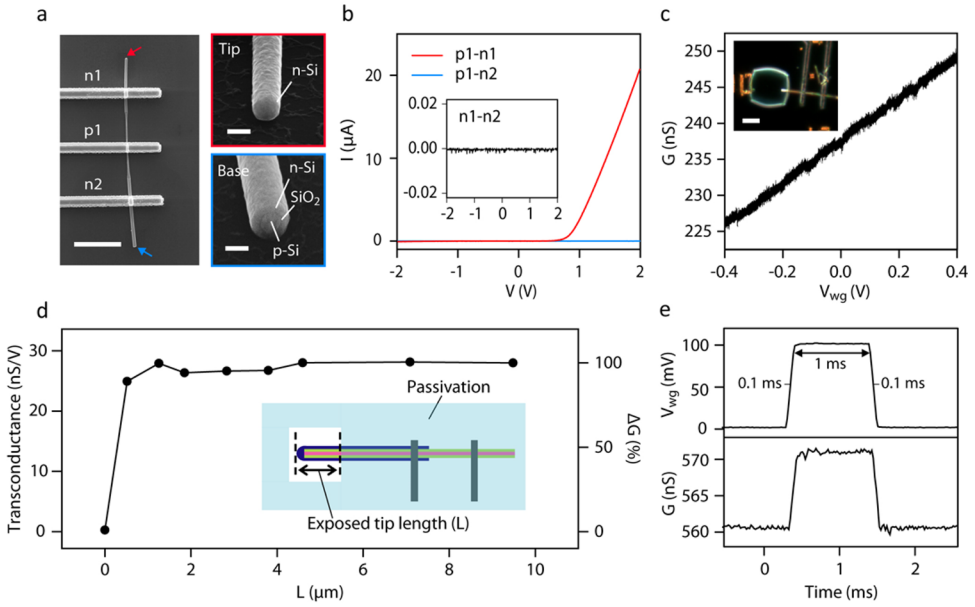

Figure 2. Electrical characterization of tip-modulated nanowire devices. (a) SEM images of a fabricated tip-modulated single nanowire device. Left: SEM image of the single nanowire device with electrical contacts for core (p1), tip end shell (n1), and base end shell (n2). Scale bar, 5 μm. Right: high-magnification SEM image of the tip end (red arrow, top) and base end (blue arrow, bottom) of the same device. Scale bars, 200 nm. (b) Measured current−voltage (I−V) curves between the core-tip end shell (p1−n1), core-base end shell (p1−n2), and tip end shell-base end shell (n1−n2, inset) contacts. The current was measured between the two contacts with the device source-drain voltage (V) swept from −2 to 2 V. (c) Measured conductance (G) of a tip-modulated nanowire device with water-gate voltage (V_{wg}) swept from −0.4 to 0.4 V. The V_{wg} was applied using a Ag/AgCl reference electrode while the device was partially covered by 1× phosphate buffer saline solution and forward biased at 1.5 V. Inset, optical microscope image of the device with the PMMA passivation layer. The nanowire tip length in the exposed window was ∼1.3 μm. Scale bar, 5 μm. (d) Measured water-gate transconductance (left axis) of a tip-modulated nanowire device with different exposed nanowire tip lengths (L). Forward bias of 1.5 V was applied. The transconductance values are normalized (right axis) with respect to that measured at L = 9.5 μm (28.0 nS/V = 100%). Inset, schematic showing the exposed nanowire tip length and passivation configuration. (e) Pulsed water-gate response of a tip-modulated nanowire device (bottom) to the applied water-gate pulse with a rise/fall time of 0.1 ms, duration of 1 ms and amplitude of 100 mV (top). Forward bias of 1.5 V was applied. The exposed tip length was ∼1.2 μm. Response from metal contacts was removed in the response graph. The devices characterized in (d,e) are different.

Measured current−voltage (I−V) curves for the single nanowire device with electrical contacts to p-core (p1), tip end n-shell (n1), and base end shell (n2) (Figure 2b) show several key features. First, the I−V data between p1−n1 (red curve) showed diode-like characteristics with very low currents in reverse bias and onset of current flow in forward bias around 0.90 V. Second, no measurable current was observed for I−V data recorded between p1−n2 (blue curve) and n1−n2 (black curve, Figure 2b, inset). These p1−n2 and n1−n2 I−V data show that the SiO_2 layer between nanowire p-core and n-shell serves as a good electrical insulator, and that our etching procedure for making the p-core contact removes the n-shell in this region of the nanowire. These results together with the observations from SEM images suggest that the rectifying p−n junction is formed at the nanowire tip end.

To illuminate further the spatial location of the p−n junction, we have carried out water-gate experiments[7−10] with variable-size masks used to change the length of the nanowire exposed to the varying solution potential. In these measurements, a length of the nanowire device near the tip was exposed to an electrolyte solution that served as the gate, while the remainder of the device was covered by a poly(methyl methacrylate) (PMMA) passivation layer (Figure 2c, see Materials and Methods in Supporting Information). For a window size of 9.5 × 9.5 μm^2 (Figure 2c, inset), ca. 1.3 μm of the nanowire tip is exposed and the conductance versus water-gate data (Figure 2c) exhibits an n-type response and a transconductance of 28.0 nS/V. To assess the spatial localization of the p−n tip junction "sensor", we measured the water-gate transconductance of the same nanowire device for different size windows (Figure 2d, see Materials and Methods in Supporting Information), where the length of the exposed nanowire tip varied from 0.5 to 9.5 μm. For an exposed tip length of 9.5 μm, the measured transconductance was 28.0 nS/V, which is similar to the transconductance for an exposed tip length of 1.3 μm. When the PMMA fully passivated the nanowire device including the tip, corresponding to L = 0 μm, the conductance change over the −0.4 to 0.4 V water-gate voltage sweep was indistinguishable from the conductance noise level of ∼2 nS. When only a 0.5 μm length including the p−n nanowire tip is exposed these measurements revealed that ∼90% of maximum transconductance is obtained. Hence, we can conclude that device sensitivity is localized to at least 500 nm of the tip, which are similar to previous reports of localized sensitivity near a p−n junction within a kinked nanowire device.[10]

In addition, we characterized the temporal response of our tip-modulated nanowire devices in aqueous solution by monitoring the time-dependent conductance change in response to V_{wg} pulses[8,9] with 0.1 ms rise/fall times, 1 ms duration, and 100 mV amplitude. The measured conductance change (Figure 2e) follows the V_{wg} pulse rise/fall without detectable broadening after the capacitive response of the passivated metal contacts was removed by standard subtraction.[9] Taken together, the electrical characterization results show that the p−n junction of our tip-modulated nanowire exhibits expected diode-like electrical characteristics and can

DOI: 10.1021/acs.nanolett.6b02236
Nano Lett. 2016, 16, 4713−4719

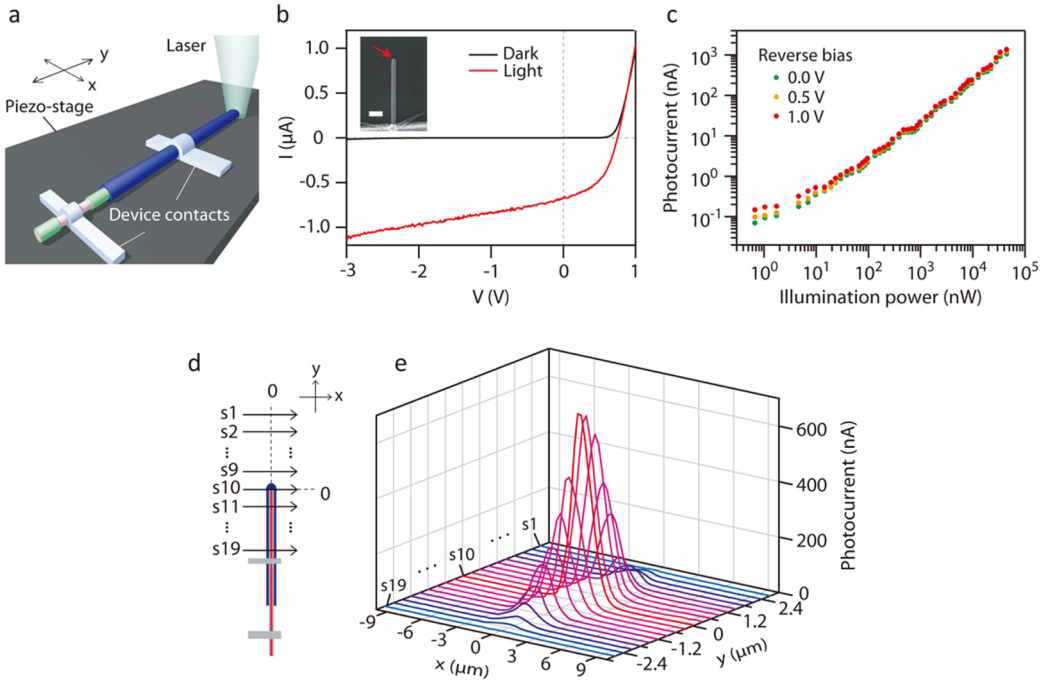

Figure 3. Optical characterization of tip-modulated nanowire devices. (a) Schematic showing a tip-modulated nanowire device mounted on a piezo-controlled movable stage and a laser focused on the nanowire tip (wavelength 488 nm, spot size ~1.6 μm). (b) Dark and light $I-V$ curves with the laser spot focused on the nanowire tip. The incident illumination power on the nanowire was ~28.1 μW. Inset, SEM image of the nanowire device on Si_3N_4 substrate with the red arrow indicating the nanowire tip. Scale bar, 1 μm. (c) Measured photocurrent as a function of incident illumination power at reverse bias voltages of 0 (green), 0.5 (orange), and 1.0 V (red). (d,e) Spatially resolved photocurrent measurements. (d) Schematic showing the line-scans in the x-direction across the nanowire. Line-scans (s1–s19) span the nanowire tip with a 300 nm step size in both x- and y-directions. (e) Measured scanning photocurrents around the nanowire tip, where the origin of the x- and y-axes is set at the nanowire tip. The incident illumination power was ~28.1 μW for all line-scans.

function as a potentiometric aqueous solution biological/chemical sensor with the device sensitivity localized at the nanowire tip and response time of at least 0.1 ms.

We have also carried out spatially resolved photocurrent measurements to investigate the capabilities of the tip-modulated nanowire p–n junctions to serve as localized nanoscale photodetectors (Figure 3a).[12,25] Tip-modulated nanowire devices were fabricated in a similar manner as described above (see Materials and Methods in Supporting Information), and scanned using piezo-controlled $x-y$ stage with a fixed Ar-ion laser excitation source (488 nm) focused to a spot size of ~1.6 μm on the device substrate surface. The incident illumination power on the nanowire was obtained by considering the area fraction of the nanowire within the laser spot when the nanowire tip is aligned to the center of the laser spot. Measurements of the basic $I-V$ characteristics (Figure 3b) show that with illumination (red curve) the device exhibits an open-circuit voltage (V_{OC}) of 0.75 V and short-circuit current (I_{SC}) of 674 nA at an incident illumination power of ~28.1 μW (see Materials and Methods in Supporting Information). We note the relatively high V_{OC} of 0.75 V results from the use of higher incident illumination power compared to previously reported axial[13] and core/shell[15] Si nanowire p–n junctions photovoltaic devices. Studies of the photocurrent versus incident illumination powers from ~1 nW to ~45 μW at 0 V (green), and reverse biases of 0.5 V (yellow) and 1 V (red) (Figure 3c) exhibit a linear response for incident illumination powers >10 nW and measurable changes down to ~1 nW. In addition, larger photocurrents are observed at larger reverse bias voltages for a given illumination power. We also estimated the responsivity (Supporting Information Figure S4), which is defined as the ratio of the measured photocurrent to the incident illumination power, to characterize the light sensitivity of the tip-modulated nanowire devices. The maximum responsivity of ~0.22 A/W was obtained at an incident illumination power of 0.7 nW and a reverse bias voltage of 1.0 V.

The photocurrent and responsivity data are consistent with previous observations for the axially and radially modulated p–n and p–i–n junction nanowire devices.[12−14] In particular, the increased photocurrent and responsivity at a larger reverse bias voltages can be attributed to improved charge collection efficiency[11] in the p–n junction as reported previously for nanowire photodetectors.[12] In addition, the reduced responsivity with increasing incident illumination power can be attributed to the thermal effect by focused illumination spot on the nanoscale p–n junction.[11] We note that the maximum responsivity of ~0.22 A/W in our tip-modulated nanowire photodetector is two orders larger than the reported value of the responsivity for a 20 nm Si p–i–n junction nanowire photodetector (with responsivity on the order of mA/W).[12] The large responsivity of our nanowire device having a diameter of 270 nm compared to the previous Si p–i–n junction nanowire photodetector with a diameter of 20 nm[12] can be attributed to the enhanced light absorption efficiency[26,27] in our device. For example, in our previous studies the absorption efficiencies of Si nanowires with two different diameters of 260 and 30 nm were calculated as ~0.84 and ~0.01, respectively.[27]

DOI: 10.1021/acs.nanolett.6b02236
Nano Lett. 2016, 16, 4713–4719

Scanning photocurrent measurements were performed to investigate the spatial dependence of the photocurrent generation as shown schematically in Figure 3d. Photocurrent scans obtained while the nanowire device was raster scanned (scanned in x perpendicular to the nanowire axis; stepped in y parallel to the axis) relative to a focused laser (Figure 3e) highlight several key points. First, as the x-scans approach from above and then reach through the nanowire tip (scans s1−s10), the photocurrent rapidly reaches the maximum value of ∼680 nA at the tip; that is, y-scan s10 with x-scan position of the nanowire axis (x = 0). Second, as the y-scans continued to increment along the nanowire axis away from the tip there is a sharp decrease in the maximum photocurrent (s11−s19). For instance, when the scan is 2.4 μm away from the tip (s18), the photocurrent decreases to about 2% of that measured at the tip. In addition, scans on the core/shell (Supporting Information Figure S5, s20) and core only (Supporting Information Figure S5, s21) regions of the device, which are 7.8 and 9.2 μm in y-direction from the tip, produce less than 0.05 and 0.02%, respectively, of the maximum photocurrent. To investigate further localized photocurrent generation at the tip, we also fabricated an optically opaque mask[14] (Supporting Information Figure S6a,b, see Materials and Methods in Supporting Information) using the same device from Figure 3. Notably, photocurrents from the masked device measured at bias voltages ranging from −3 to 0 V decreased to less than 4% of the photocurrents observed prior to tip-masking (Supporting Information Figure S6c) while the dark I−V curves remained similar before and after tip-masking. Taken together, these studies demonstrate that the localized p−n junction of our tip-modulated nanowire serves as an efficient photodetector with photocurrent generation localized at the nanowire tip.

In addition, we have explored a hybrid top-down/bottom-up synthetic approach to prepare large arrays of tip-modulated nanowires. SEM images (Figure 4a) reveal the nanowire morphology following key steps of our hybrid approach. First, deep reactive ion etching through an SU-8 patterned mask on a p-Si wafer followed by oxygen plasma cleaning to remove remaining SU-8 (see Materials and Methods in Supporting Information) yields vertical micropillars[28] arrays with diameters of ca. 1.2 μm and lengths of 18 μm (Figure 4a, I). Second, KOH wet-etching step was used to reduce pillar diameters to ca. 300−400 nm (Figure 4a, II). Third, a conformal shell of SiO_2 was deposited by ALD (Figure 4a, III), and a 20 μm thick SU-8 protective resist was spun on the wafer. Oxygen plasma was used to remove SU-8 and expose the nanowire tips, and then the wafer was dipped into ultrasonication bath. SEM images (Supporting Information Figure S7) show clearly arrays of exposed nanowire tips, oxygen plasma thinning of the SU-8, and the removal of these tips following the ultrasonication step. The remaining SU-8 was removed as described above, the wafer was briefly cleaned with BHF, and then the n-Si shell was deposited in the CVD reactor to yield arrays of vertical p−n junction tip-modulated nanowires (Figure 4a, IV).

Larger area SEM images (Figure 4b−d) highlight the capabilities of this hybrid approach. First, an overview image (Figure 4b) shows a 1.5 × 1.5 mm^2 area containing of 25 tiles (5 × 5 array), where each tile contains an array of the tip-junction nanowires. A higher-magnification SEM image (Figure 4c) of 4 tiles (red box in Figure 4b) exhibits a uniform distribution of nanowires in each tile. In addition, a representative tilted-view SEM image of one tile (Figure 4d) highlights the 15 × 15 array of vertical tip-junction nanowires.

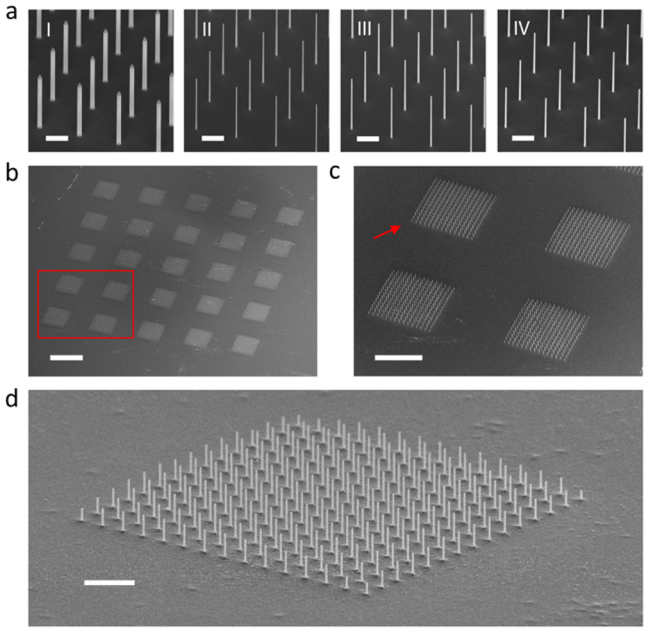

Figure 4. Large-scale synthesis of vertical tip-modulated nanowire arrays. (a) SEM images (45° tilt) following steps of the top-down/bottom-up synthesis of vertical tip-modulated nanowire arrays: (I) deep reactive ion etching of p-Si (111) wafer; (II) KOH wet etching to reduce the diameter of the p-Si core micropillars; (III) deposition of 100 nm SiO_2 by ALD; and (IV) removal of the tips through ultrasonication and n-Si shell growth by CVD. Scale bars, 5 μm. (b−d) SEM images of as-synthesized vertical tip-modulated nanowire arrays. (b) Low-magnification SEM image (45° tilt) of 25 tiles of 15 × 15 tip-modulated nanowire arrays. Scale bar, 200 μm. (c) SEM image of the nanowire tiles in the red box in (b). Scale bar, 100 μm. (d) High-angle SEM image (70° tilt) of a 15 × 15 nanowire tile (the red arrow in (c)). Scale bar, 20 μm.

Inspection of this and similar images shows that most of the nanowires have a uniform length expected from the hybrid approach, although some nanowires at the array corners are shorter than expected; only nanowires with expected lengths (>10 μm) are considered as successful in our yield calculations. We find at least 4300 vertical tip-junction nanowires meet this criteria for a final synthetic yield of >75% from ∼5600 mask sites defined in the initial lithographic and RIE etching steps. Hence, we conclude that this hybrid approach is an effective synthetic route for large-scale production of the tip-modulated nanowires.

To explore the functional behavior of p−n junction tip-modulated nanowires prepared by the hybrid approach, we have fabricated addressable nanowire devices as shown schematically in Figure 5 (see Materials and Methods in Supporting Information). First, an array of tip-modulated nanowires was fabricated over an area of >20 mm^2 on a p-Si wafer as described above. We then assign a group of four vertical nanowires as a single device during the fabrication of the device arrays. A cross-section of two nanowires is highlighted in the fabrication scheme (Figure 5a, I) for clarity. Photolithography is then used to define an etch mask with area and thickness greater than the footprint and length, respectively, of the subset of four nanowires in each device (Figure 5a, II), and aqueous KOH solution is used to n-Si layer in the surrounding regions (Figure 5a, III) to isolate the n-Si shell of the nanowire devices. Last, we use photolithography and metal deposition to define a common core contact,

DOI: 10.1021/acs.nanolett.6b02236
Nano Lett. 2016, 16, 4713−4719

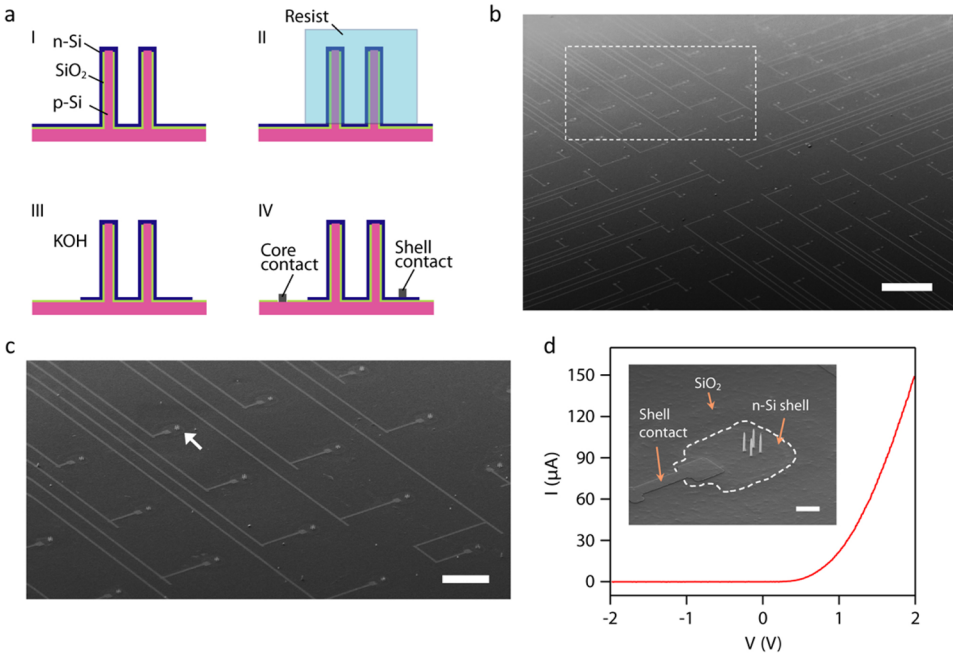

Figure 5. Vertical tip-modulated nanowire device array. (a) Schematics of device fabrication on subset of nanowires: (I) p-Si cores and substrate coated with SiO_2 and n-Si shell using bottom-up/top-down approach of Figure 4; (II) SU-8 resist patterned using photolithography on a single subset of nanowires to serve as etch mask; (III) KOH wet etching to remove the n-Si shell not covered by SU-8 resist; (IV) partial removal of SiO_2 insulation layer using BHF to expose the p-Si substrate, and thermal evaporation of metal contacts to the common p-Si core and individually addressable n-shells. (b) SEM image (60° tilt) of vertical tip-modulated nanowire device array in 10 × 10 grid layout. Scale bar, 500 μm. (c) Higher-magnification SEM image of white dotted box in (b). The common core contact is not shown in this image. Scale bar, 200 μm. (d) $I-V$ curve recorded from a single-unit device indicated by the white arrow in (c). Inset, magnified SEM image of the single-unit device consisting of 2 × 2 array of vertical tip-modulated nanowires. The white dashed line indicates the n-Si shell/layer region that was not removed by KOH etching. Scale bar, 20 μm.

individual device shell contacts, and interconnect lines (Figure 5a; IV).

Following fabrication, an SEM image (Figure 5b) highlights the 100 single-unit devices, each consisting of 4 tip-modulated nanowires, in a 10 × 10 grid layout distributed over an area of >20 mm^2. A magnified SEM image (Figure 5c) from the white box in Figure 5b shows the individual n-Si shell contacts and corresponding nanowire single-unit devices. Electrical transport data recorded from a representative working single-unit 4-nanowire device (Figure 5d) exhibit diode-like $I-V$ characteristics (Figure 5d) with turn-on voltage of ca. 1.0 V, which is similar to those from single tip-modulated p−n junction nanowires (e.g., Figure 2b). The forward bias current at 1.5 V, ∼150 μA, is larger than that current from the bottom-up synthesized single nanowire device in Figure 2b. The higher current can be explained by the larger junction area per nanowire, which is due to the larger diameters of the hybrid versus bottom-up nanowires, and the four nanowires in a single device. We measured electrical transport properties for all 100 devices in Figure 5b and found that 56/100 devices exhibited diode-like characteristics. We believe that modest yield can be attributed in large part to breakage of vertical nanowires during multiple photolithography, thermal evaporation, and lift-off steps, and believe that optimizing this fabrication should enable improvements in the future. Even at the current yield levels, the p−n junction tip-modulated vertical nanowire device arrays can be useful for large area and independently addressable optical and electrical signal detection given that the active device sensor regions are localized substantially above the 2D plane of the device chip.

In summary, we have proposed and demonstrated an approach for the synthesis of tip-modulated nanowires by synthetically encoding a localized nanoscale p−n junction at nanowire tips. SEM and TEM imaging verified that the designed p-Si nanowire core with SiO_2 insulating inner shell and n-Si outer shell with clean p-Si/n-Si tip junction, and electrical transport measurements with independent contacts to the p-Si core and n-Si shell demonstrated current rectification behavior through the tip junction without detectable current through the SiO_2 shell. Electrical measurements also showed an n-type response in conductance versus water-gate voltage with pulsed gate experiments yielding a temporal resolution of at least 0.1 ms, and a ∼90% device sensitivity localized to within 0.5 μm from the nanowire p−n tip. In addition, photocurrent experiments exhibited linear dependence of photocurrent with respect to incident illumination power, an estimated responsivity up to ∼0.22 A/W at reverse bias of 1.0 V with 28.1 μW illumination power, and a photocurrent peak at the tip of nanowire in spatially resolved measurements. In addition, tip-modulated junction concept was further extended to a top-down/bottom-up hybrid approach that enabled large-scale production of vertical tip-modulated nanowires with a final synthetic yield of >75% for thousands of nanowires. Individually addressable nanowire device arrays fabricated using this hybrid approach yielded devices exhibiting diode-like current−voltage characteristics. In the future, we believe that the tip-modulated Si nanowire devices can be used for multiplexed detection of electrical, chemical, and optical signals in biological systems and, moreover, that the tip-modulated structure can be generalized to other material combinations, including Si/III−V,[29−31] Si/II−VI[32] and III−V/III−V,[33,34] to

DOI: 10.1021/acs.nanolett.6b02236
Nano Lett. 2016, 16, 4713−4719

spatially encode a distinct type of device functionality that could be useful for applications in nanoelectronics, quantum electronics, and optoelectronics.

■ ASSOCIATED CONTENT

Supporting Information

The Supporting Information is available free of charge on the ACS Publications website at DOI: 10.1021/acs.nanolett.6b02236.

Detailed description of experimental methods and additional figures.(PDF)

■ AUTHOR INFORMATION

Corresponding Authors

*E-mail: hgpark@korea.ac.kr.

*E-mail: cml@cmliris.harvard.edu.

Author Contributions

Y.-S.N. and R.G. have contributed equally to this manuscript.

Notes

The authors declare no competing financial interest.

■ ACKNOWLEDGMENTS

We thank N. Antoniou for assistance with the focused ion beam. C.M.L. acknowledges the support from the Air Force Office of Scientific Research (AFOSR, FA9550-15-1-0401). R.G. acknowledges the support of Japan Student Services Organization Graduate Research Fellowship. M.N.M. acknowledges a Fannie and John Hertz Foundation Graduate Fellowship and an NSF Graduate Research Fellowship. R.W.D. acknowledges an NSF Graduate Research Fellowship. H.-G.P. acknowledges support by the National Research Foundation of Korea (NRF) grant funded by the Korean government (MSIP) (No. 2009-0081565).

■ REFERENCES

(1) Lieber, C. M. *MRS Bull.* **2011**, *36*, 1052−1063.

(2) Hayden, O.; Agarwal, R.; Lieber, C. M. *Nat. Mater.* **2006**, *5*, 352−356.

(3) Yan, R. X.; Park, J. H.; Choi, Y.; Heo, C. J.; Yang, S. M.; Lee, L. P.; Yang, P. D. *Nat. Nanotechnol.* **2011**, *7*, 191−196.

(4) Xie, C.; Lin, Z. L.; Hanson, L.; Cui, Y.; Cui, B. *Nat. Nanotechnol.* **2012**, *7*, 185−190.

(5) Zimmerman, J. F.; Murray, G. F.; Wang, Y.; Jumper, J. M.; Austin, J. R., II; Tian, B. Z. *Nano Lett.* **2015**, *15*, 5492−5498.

(6) Xu, L.; Jiang, Z.; Mai, L.; Qing, Q. *Nano Lett.* **2014**, *14*, 3602−3607.

(7) Tian, B. Z.; Cohen-Karni, T.; Qing, Q.; Duan, X.; Xie, P.; Lieber, C. M. *Science* **2010**, *329*, 830−834.

(8) Duan, X. J.; Gao, R. X.; Xie, P.; Cohen-Karni, T.; Qing, Q.; Choe, H. S.; Tian, B. Z.; Jiang, X. C.; Lieber, C. M. *Nat. Nanotechnol.* **2011**, *7*, 174−179.

(9) Fu, T.-M.; Duan, X.; Jiang, Z.; Dai, X.; Xie, P.; Cheng, Z.; Lieber, C. M. *Proc. Natl. Acad. Sci. U. S. A.* **2014**, *111*, 1259−1264.

(10) Jiang, Z.; Qing, Q.; Xie, P.; Gao, R. X.; Lieber, C. M. *Nano Lett.* **2012**, *12*, 1711−1716.

(11) Sze, S. M. *Physics of Semiconductor Devices*; Wiley: New York, 1981; pp 63−132, 743−789.

(12) Yang, C.; Barrelet, C. J.; Capasso, F.; Lieber, C. M. *Nano Lett.* **2006**, *6*, 2929−2934.

(13) Kempa, T. J.; Tian, B. Z.; Kim, D. R.; Hu, J. S.; Zheng, X. L.; Lieber, C. M. *Nano Lett.* **2008**, *8*, 3456−3460.

(14) Tian, B. Z.; Zheng, X. L.; Kempa, T. J.; Fang, Y.; Yu, N. F.; Yu, G. H.; Huang, J. L.; Lieber, C. M. *Nature* **2007**, *449*, 885−889.

(15) Kempa, T. J.; Cahoon, J. F.; Kim, S. K.; Day, R. W.; Bell, D. C.; Park, H. G.; Lieber, C. M. *Proc. Natl. Acad. Sci. U. S. A.* **2012**, *109*, 1407−1412.

(16) Kim, S. K.; Day, R. W.; Cahoon, J. F.; Kempa, T. J.; Song, K. D.; Park, H. G.; Lieber, C. M. *Nano Lett.* **2012**, *12*, 4971−4976.

(17) Krogstrup, P.; Jorgensen, H. I.; Heiss, M.; Demichel, O.; Holm, J. V.; Aagesen, M.; Nygard, J.; Fontcuberta i Morral, A. *Nat. Photonics* **2013**, *7*, 306−310.

(18) Gudiksen, M. S.; Lauhon, L. J.; Wang, J.; Smith, D. C.; Lieber, C. M. *Nature* **2002**, *415*, 617−620.

(19) Yao, M.; Huang, N.; Cong, S.; Chi, C.-Y.; Seyedi, M. A.; Lin, Y.-T.; Cao, Y.; Povinelli, M. L.; Dapkus, P. D.; Zhou, C. *Nano Lett.* **2014**, *14*, 3293−3303.

(20) Thompson, M. D.; Alhodaib, A.; Craig, A. P.; Robson, A.; Aziz, A.; Krier, A.; Svensson, J.; Wernersson, L.-E.; Sanchez, A. M.; Marshall, A. R. J. *Nano Lett.* **2016**, *16*, 182−187.

(21) Lauhon, L. J.; Gudiksen, M. S.; Wang, C. L.; Lieber, C. M. *Nature* **2002**, *420*, 57−61.

(22) Wagner, R. S.; Ellis, W. C. *Appl. Phys. Lett.* **1964**, *4*, 89−90.

(23) Schmid, H.; Bjork, M. T.; Knoch, J.; Riel, H.; Riess, W.; Rice, P.; Topuria, T. *J. Appl. Phys.* **2008**, *103*, 024304.

(24) Woodruff, J. H.; Ratchford, J. B.; Goldthorpe, I. A.; McIntyre, P. C.; Chidsey, C. E. D. *Nano Lett.* **2007**, *7*, 1637−1642.

(25) Barnard, E. S.; Pala, R. A.; Brongersma, M. L. *Nat. Nanotechnol.* **2011**, *6*, 588−593.

(26) Cao, L.; White, J. S.; Park, J.-S.; Schuller, J. A.; Clemens, B. M.; Brongersma, M. L. *Nat. Mater.* **2009**, *8*, 643−647.

(27) Day, R. W.; Mankin, M. N.; Gao, R.; No, Y. S.; Kim, S. K.; Bell, D. C.; Park, H. G.; Lieber, C. M. *Nat. Nanotechnol.* **2015**, *10*, 345−352.

(28) Park, H.; Dan, Y.; Seo, K.; Yu, Y. J.; Duane, P. K.; Wober, M.; Crozier, K. B. *Nano Lett.* **2014**, *14*, 1804−1809.

(29) Munshi, A. M.; Dheeraj, D. L.; Fauske, V. T.; Kim, D. C.; Huh, J.; Reinertsen, J. F.; Ahtapodov, L.; Lee, K. D.; Heidari, B.; van Helvoort, A. T. J.; Fimland, B. O.; Weman, H. *Nano Lett.* **2014**, *14*, 960−966.

(30) Hocevar, M.; Immink, G.; Verheijen, M.; Akopian, N.; Zwiller, V.; Kouwenhoven, L.; Bakkers, E. *Nat. Commun.* **2012**, *3*, 1266.

(31) Borg, M.; Schmid, H.; Moselund, K. E.; Signorello, G.; Gignac, L.; Bruley, J.; Breslin, C.; Kanungo, P. D.; Werner, P.; Riel, H. *Nano Lett.* **2014**, *14*, 1914−1920.

(32) Mankin, M.; Day, R.; Gao, R.; No, Y.-S.; Kim, S.-K.; McClelland, A.; Bell, D.; Park, H.-G.; Lieber, C. M. *Nano Lett.* **2015**, *15*, 4776−4782.

(33) Wallentin, J.; Anttu, N.; Asoli, D.; Huffman, M.; Aberg, I.; Magnusson, M. H.; Siefer, G.; Fuss-Kailuweit, P.; Dimroth, F.; Witzigmann, B.; Xu, H. Q.; Samuelson, L.; Deppert, K.; Borgstrom, M. T. *Science* **2013**, *339*, 1057−1060.

(34) Heiss, M.; Fontana, Y.; Gustafsson, A.; Wust, G.; Magen, C.; O'Regan, D. D.; Luo, J. W.; Ketterer, B.; Conesa-Boj, S.; Kuhlmann, A. V.; Houel, J.; Russo-Averchi, E.; Morante, J. R.; Cantoni, M.; Marzari, N.; Arbiol, J.; Zunger, A.; Warburton, R. J.; Fontcuberta i Morral, A. *Nat. Mater.* **2013**, *12*, 439−444.

DOI: 10.1021/acs.nanolett.6b02236
Nano Lett. 2016, 16, 4713−4719